Ensemble Bayesian Neural Nowcasting of Geostationary Multispectral Imagery For Hydro-Meteorological Applications

M. de Rosa, F.S. Marzano, G. Rivolta and A. Eleuteri

***Abstract*—Many severe meteorological events develop at short time scales. The availability of effective rain-rate nowcasting techniques is valuable for Civil Protection purposes. Neural network based nowcasting techniques, exploiting satellite data, have been proven to be more accurate than conventional techniques. The objective of this work is to explore possible improvements of the neural-network approach named Neural Combined Algorithm for Storm Tracking (NeuCAST). In its single channel version (developed for Meteosat-7) this technique has been successfully applied, using feed-forward (FF) and recurrent (RC) neural networks, to the rainfall field nowcast from thermal infrared (TIR) and microwave (MW) passive-sensor imagery aboard, respectively, Geostationary-Earth-Orbit (GEO) and Low-Earth-Orbit (LEO) satellites.**

This work proposes a new version of the NeuCAST technique, named Generalized Combined Algorithm for Storm Tracking (GenCAST), based on the Generalized Linear Model (GLM), and the introduction of the Ensemble Bayesian approach in the GenCAST technique extended to infrared (IR) multi-channel data available from Meteosat Second Generation (MSG). The ensemble approach here proposed is named DAN (Dynamically Averaging Networks). Such approach differs from the typical ensemble approach in that the weights, used to compute the ensemble output, are dynamically updated rather than being a priori determined. The reason of such choice is that ensemble of models properly trained over a sufficiently representative dataset can widen the response variety to a certain input pattern allowing the selection of the input/output pattern associated with the highest likelihood with respect to the latest available data. The proposed method to determine the dynamic weights is discussed. Several applications of the DAN ensemble approach to the multi-channel GenCAST, related to different case studies over Southern Europe in 2006-2010, are presented and relevant results are discussed.

Frank S. Marzano and Michele de Rosa are with the Dept. of Electronic Engineering, Sapienza University of Rome, Via Eudossiana 18 – 00184 Rome, Italy and with the Center of Excellence CETEMPS, University of L'Aquila (e-mail: marzano@die.uniroma1.it).

Michele de Rosa is with the T.R.S. S.p.A via della Bufalotta, 378 – 00139 Rome, Italy (email: mic_der@yahoo.it).

Giancarlo Rivolta is with the European Space Agency (ESA) - ESRIN (EOP-GTR), Casella Postale 64, 00044 Frascati (RM), Italy (e-mail: giancarlo.rivolta@esa.int).

A. Eleuteri is with the Department of Clinical Engineering, Royal Liverpool & Broadgreen University Hospitals NHS Trust (RLBUHT) and the University of Liverpool, Prescot Street, L7 8XP, Liverpool, UK (e-mail: antonio.eleuteri@gmail.com)

Corresponding author: M. de Rosa, tel +39.3283418614, e-mail mic_der@yahoo.it.

***Index Terms*— Satellite meteorology, Nowcasting applications, Neural networks, Generalized Linear Model, Bayesian estimation, Ensemble techniques.**

I. Introduction

NOWCASTING of rainfall from remote sensing imagery is becoming an important issue for several applications, which are mainly related to civil protection alarming and also to hydro-meteorological applications [1]-[4]. Multiple scales of space and time can be taken into account, as well as different data sources and objectives. The term nowcast should be intended, in this context, as the ability to predict, at very short-term time scales, the evolution of the geophysical field of interest from remote sensing imagery. The satellite measurements used here implicitly define the time and space sampling imposed by the involved platform and sensor features [5]-[7].

For a rapidly varying field, such as rainfall, high temporal repetition of the observation, like that available from geostationary satellites, is essential [8]. On the other hand, the accuracy of the nowcasted fields is strictly related to the physical correlation of the measured remotely sensed data with the field of interest [9]-[11]. The rainfall nowcast problem from the satellite remote passive sensors can be conveniently split into two basic components as follows: 1) instantaneous retrieval; and 2) temporal prediction.

Several rain retrieval techniques have been proposed on the basis of multi-satellite imagery, exploiting passive sensor measurements acquired by geostationary Earth orbit (GEO) and low Earth orbit (LEO) platforms [8]-[14]. These approaches tend to overcome some inherent limitations due to the use of satellite infrared (IR) radiances, which are poorly correlated with rainfall [6]. In this respect, microwave (MW) radiometric data available from LEO platforms can provide more accurate rain estimates [15]. From a microphysical point of view, visible (VIS) and IR radiometers can give information on cloud top layers since precipitating clouds are almost completely opaque are in the IR. On the other hand, MW radiometers can detect cloud structure and, to some extent, near-surface rainfall. In fact, MW brightness temperatures are fairly sensitive to liquid and ice hydrometeors since rain clouds are not optically opaque at MW frequencies [16]. From

a system point of view, GEO satellites can ensure an Earth coverage with a high temporal sampling, whereas LEO satellites have the advantage to enable the use of MW sensors but with the drawback of low temporal sampling. Therefore, LEO-MW and GEO-IR radiometries are clearly complementary in monitoring the Earth's atmosphere and a highly variable phenomenon such as precipitation. The IR radiances from geostationary images can be properly calibrated using the MW-based combined algorithms (e.g., [5] and [13]-[16]). Microwave data can be extracted from the MW imager sensors, but any rain estimation source may be used [9]. Rainfall nowcasting by active and passive remote sensing imagery has been attempted by numerous techniques in the last decade [3], [4], [17], [18]. Some of the proposed nowcast methods may be classified as standard, which are, hereafter, also called "conventional," such as the temporal image persistence (TIP) and steady-state displacement (SSD) (e.g., [17]). Each of these conventional nowcasting methods shows a performance that depends on the weather conditions in the considered region.

The ensemble technique is a consolidated framework used to mediate between the outputs of different models. It has been shown that the output of an ensemble minimizes the average sum-of-square error [19].

The basic aim of this paper is to exploit the potential of the ensemble technique to both predict and retrieve the rainfall pattern, having at disposal both GEO-IR and LEO-MW passive sensor data. The latter are provided by means of the Eumetsat Multi-sensor Precipitation Estimate (MPE) product [20]. Great attention has been placed to select the input space-time features and the optimization of the ensemble parameters in order to optimize the rainfall nowcasting performance from the satellite imagery temporal sequences with respect to the conventional approaches. The goal of the proposed technique is to describe a general ensemble technique that is flexible, general and quickly available.

II. DATA

The data related to the brightness temperature are taken from the 8 IR channels of the MSG 8/9, while the data related to the rain field are taken from the Multi-sensor Precipitation Estimate (MPE) product provided by Eumetsat [20].

A. Geostationary Satellite Data

As a source of GEO satellite imagery, the Meteosat-8/9 Spinning Enhanced Visible and InfraRed Imager (SEVIRI) has been considered here, selecting areas of interest in Southern Europe (e.g., [9]). The selected IR MSG image frames are composed of 275 × 344 pixels, corresponding roughly to east longitude ranging from 7◦ to 18◦ and north latitude ranging from 36.5◦ to 48◦ (see small panels in Fig. 1). Each SEVIRI pixel can be approximated by a square of 3 × 3 km at midlatitudes.

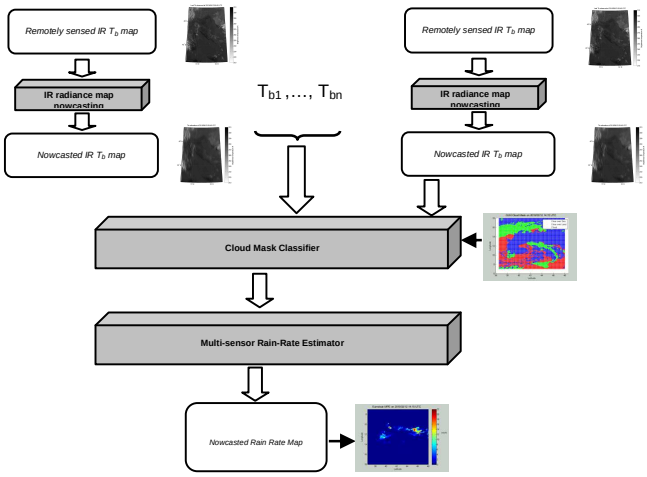

Fig. 1. The GenCAST logical layout: the flow goes from the MSG images acquisition to the rain rate estimation.

The MPE has been selected as product derived from LEO satellites. The MPE consists of the near-real-time rain rates in mm/h for each MSG image in original pixel resolution. The algorithm is based on the combination of polar orbiter microwave measurements and images in the Meteosat IR channels. The MPE is most suitable for convective precipitation.

B. The case studies

The case studies are related to some meteorological events within the Mediterranean Sea (Italy) and they are divided into two groups: the first group is used to train the model related to the MSG images (image nowcasting) and the second group considers very interesting meteorological events (like snow and thunderstorms).

The events belonging to the first group are the following:

- July 24th, 2006: training case
- August 13th, 2006: training case
- September 14th, 2006: training case
- March 20th, 2007: validation case

The first event is related to a strong thunderstorm activity over the Italy, while the other events are related to cloud motion over the Italy with heavy and moderate rain.

The events belonging to the second group are the following:

- January 26th, 2010: validation case
- February 1st,2010: validation case
- September 8th, 2010: training case

The first event is related to a winter heavy rain together with snow events over the Italy, while the second event is a snow event. Finally the third event is related to a very strong thunderstorm activity (rain rate peak over 200 mm/h).

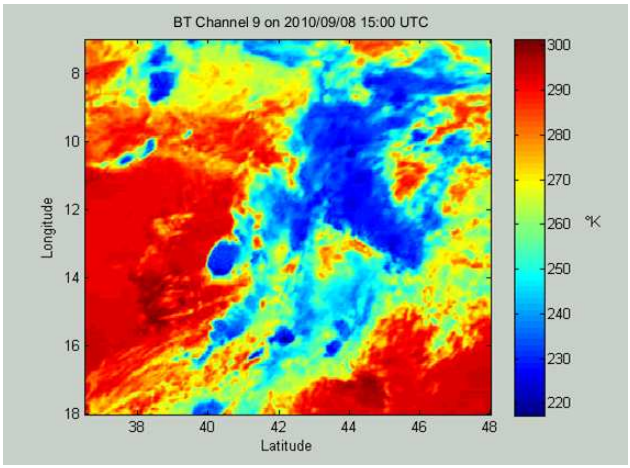

Fig. 2. The trainig case study of the second group: the MSG Channel 9 Brilliance Temperature. The image shows a thunderstorm activity over the Italy.

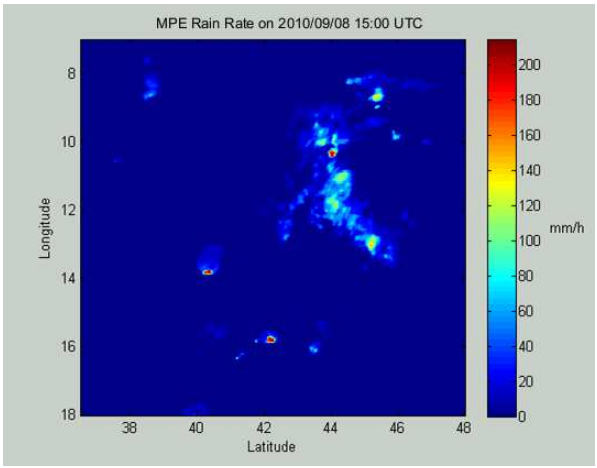

Fig. 3. The training case study of the second group: the MPE product provided by Eumetsat. The thunderstorm activity produce a 200 mm/h rain rate peak in the Tyrrhenian Sea and in the North Adriatic Sea.

III. THE METHODOLOGY

The approach followed to build the nowcasting framework, shown in Fig. 1, is bottom-up.

First of all the ensemble model has been setup in order to be used for the MSG images nowcasting from 30 minutes to 60 minutes. After a cloud classifier has been trained in order to classify each pixel of a MSG image and finally a rain rate estimator has been setup in order to estimate the rain rate on the cloudy pixels.

A. Nowcasting network architecture

The ensemble architecture chosen is shown in Fig. 4.

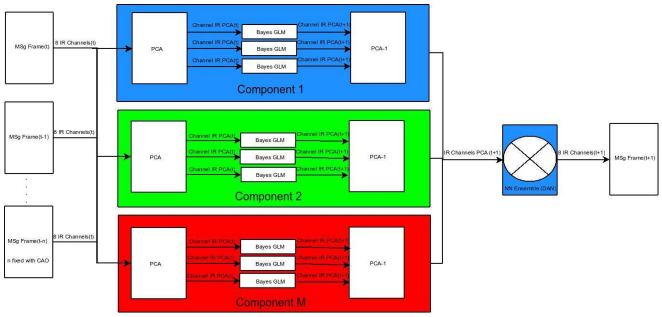

Fig. 4. The nowcasting architecture. The frames in input are broadcasted to each ensemble's components and the output of each component is mixed to give the ensemble's output.

It is clear that the ensemble paradigm is fully embedded in Fig. 4. The temporal window was found using the Cao method [21] to discover the optimal embedding dimension. This dimension is the number of images in the past related to the current frame. This number has been fixed to 6 images or 90 minutes in the past. According to it, the MSG frames are given in input to the ensemble. The MSG IR channels are compressed using the PCA [22] in order to speed-up the computation time and then dispatched to each ensemble's component. Each component is a Generalized Linear Model (GLM) [23], which is trained using the Bayesian Framework [24] and the NeuCAST's approach [25]. Each component gives its own prediction and each output is mixed following the Dynamically Average Network (DAN) approach [26].

B. Generalized Linear Models

The base model used as ensemble's components is the Generalized Linear Model (GLM) [23], which can be written in the form:

$$E(Y) = \mu = g^{-1}(\eta) \qquad \textbf{(1)}$$

The GLM generalizes linear regression by allowing the linear model to be related to the response variable via a link function g, while the other components of the models are: 1) a distribution function *f*, from the exponential family and 2) a linear predictor $\eta = \mathbf{X}\boldsymbol{\beta}$.

In a GLM, each outcome of the dependent variables, Y, is assumed to be generated from a particular distribution function in the exponential family; a large range of probability distributions that includes the normal, binomial and Poisson distributions, among others.

The model chosen sets the identity function as link and f is the Gaussian distribution. So the GLM could be written in the form:

$$y(x;w) = \sum_{j=1}^{M} w_j \phi(x_j) = W^T \Phi(X) \qquad \textbf{(2)}$$

where $\phi(x)$ is a linear function.

The Bayesian framework [24], used to train the GLM model, implements the Occam razor in order to penalize the model overall complex versus simpler models. It applies two steps, according to (3), to find the best model mapping the data:

1) Fit the model to the data. This is the training step.

2) Compute the evidence to find the best model. This is the regularization step.

$$Posterior = \frac{Likelihood \times prior}{Evidence} \quad \textbf{(3)}$$

Finally in order to minimize the amount of information regarding the IR channels a Principal Components Analisys (PCA) [22] has been applied. This technique applies a linear transformation on the data and it has the advantage of reduce the number of channels, but it is a loss of information technique, because it penalizes the components of the data which aren't representative of the data.
The error introduced by the PCA did not allow to apply the Neural Nets (NN), used in the NeuCAST, to the study, because these models are very sensitive to the errors.
The figure Fig. 5 shows the RMSE error introduced by the PCA.

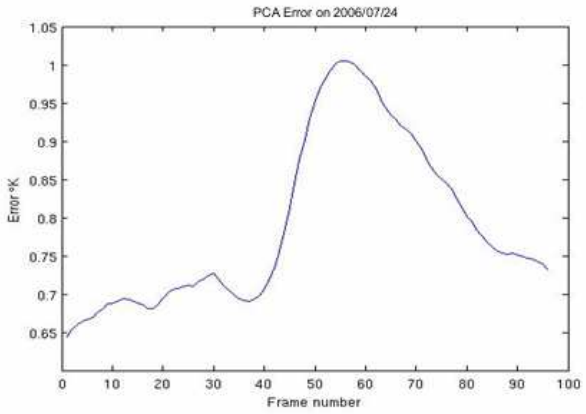

Fig. 5. The error introduced by the PCA.

C. The Ensemble nowcasting methods

The ensemble of models is a composition of different models (the ensemble's components) whose outputs are mixed to give the output of the ensemble. Given *L* components, the general form of the ensemble is the General Ensemble Model (GEM) [19][26] which has the following form:

$$f_{GEM} = \sum_{i=1}^{L} \alpha_i f_i(x) \quad \textbf{(4)}$$

In general the mixed coefficients α_i are constrained by the following conditions:

1) $0 \le \alpha_i \le 1$

and

2) $\sum_{i=1}^{L} \alpha_i = 1.$

These two conditions guarantees that the output of (4) is a weighted sum of its components.
The naive form of the GEM is the Basic Ensemble Model (BEM) which has the following form:

$$f_{BEM} = \frac{1}{n} \sum_{i=1}^{L} f_i(x) \quad \textbf{(5)}$$

It is possible to show that the average sum-of-square error introduced by the GEM and the average sum-of-square error introduced by the BEM have the relation:

$$E_{GEM} \le E_{BEM} \quad \textbf{(6)}$$

The approach used in this work is named Dynamically Averaging Networks (DAN) [26] and it is a special case of the GEM. The form of the DAN is the following:

$$f_{DAN} = \sum_{i=1}^{L} w_i f_i(x) \quad \textbf{(7)}$$

where

$$w_i = \frac{c(p_{f_i})}{\sum_{j=1}^{L} c(p_{f_j})} \quad \textbf{(8)}$$

and $c(p_{f_i})$ is the certainty function defined as follows:

$$c(p_{f_i}) = \begin{cases} p_{f_i} & \text{if } p_{f_i} \ge 0.5 \\ 1 - p_{f_i} & \text{otherwise} \end{cases} \quad \textbf{(9)}$$

In the DAN approach the parameters or weights are not fixed a priori, but are computed dynamically every time a new output appears.
To apply the DAN, it should be possible to assign a probability to each output of the ensemble's components, in order to compute the certainty function. If $Err_i(f_i)$ is the error bar related to the output of the component *i* then it should be possible to assign a probability to each output as follows:

$$p_i(f_i) = \frac{Err_i(f_i)}{\sum_{j=1}^{L} Err_j(f_j)} \quad \textbf{(10)}$$

It is possible to show [19] that:

$$1 \le E_{DAN} \le E_{GEM} + 1 \quad \textbf{(11)}$$

D. The Cloud Mask product

The Cloud Mask (CM) product is used to classify each pixel into one of the three following classes: Clear over Sea, Clear over Land and Cloud. The classes are the same as the analogous Satellite Application Facilities (SAF) CM product [27]. The model used to simulate the CM is a GLM classifier with the $\phi(x)$ function is the softmax function.

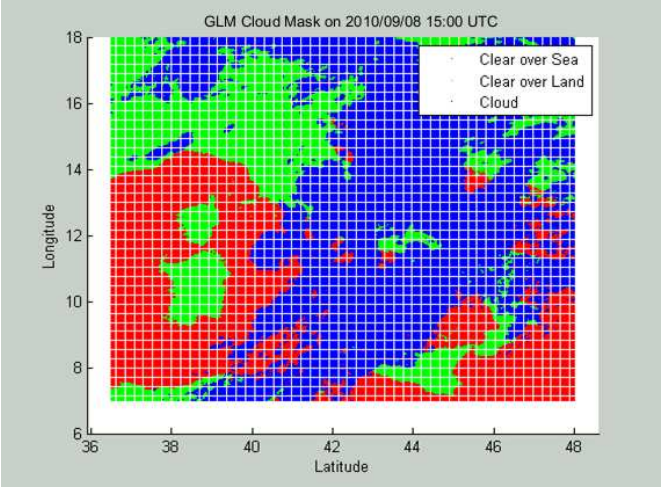

Fig. 6. The GLM Cloud Mask for one of the case studies.

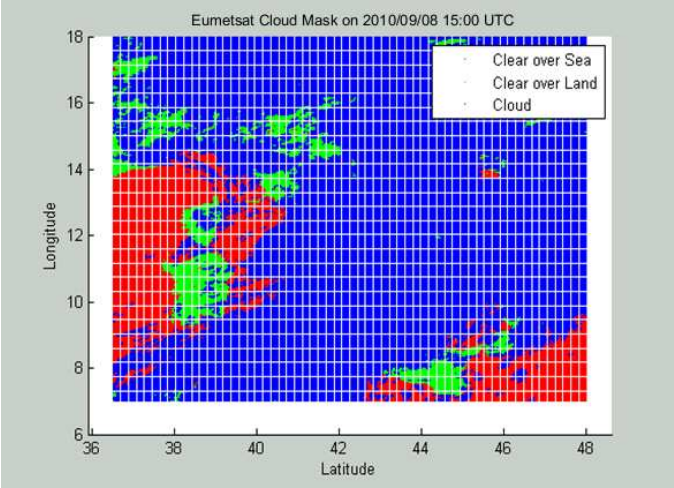

Fig. 7. The Eumetsat Cloud Musk product corresponding to one of the case studies.

IV. RESULTS

The results showed in this section are related to the case studies of the first and the second group. The results of the first group will be presented in the form of performances indexes' tables regarding the image prediction with respect to the observed image while the results of the second group will be presented in the form of the contingency matrixes of the GLM Cloud Mask with respect to the Eumetsat Cloud Mask.

A. The Performance Indexes and the Benchmarks

The performance indexes used to measure the quality of the image nowcasting are the following: the BIAS (Eq. 12), the RMSE (Eq. 13) and the Correlation Index (Eq. 14):

$$m_\varepsilon(t_k) = \frac{1}{N_{points}} \sum \left[T_b^{est}(P_i,t_k) - T_b(P_i,t_k) \right] \quad \textbf{(12)}$$

$$s_\varepsilon(t_k) = \left(\frac{1}{N_{points}} \sum \left[T_b^{est}(P_i,t_k) - T_b(P_i,t_k) \right]^2 \right)^{\frac{1}{2}} \quad \textbf{(13)}$$

$$r_\varepsilon(t_k) = \frac{\sum \left[T_b^{est}(P_i,t_k) - \left\langle T_b^{est}(t_k) \right\rangle \right] \left[T_b(P_i,t_k) - \langle T_b(t_k) \rangle \right]}{\left(\sum \left[T_b^{est}(P_i,t_k) - \left\langle T_b^{est}(t_k) \right\rangle \right]^2 \sum \left[T_b(P_i,t_k) - \langle T_b(t_k) \rangle \right]^2 \right)^{\frac{1}{2}}} \quad \textbf{(14)}$$

The benchmarks used to compare the image prediction are the Persistence [17] and the Steady State Displacement (SSD) [17]. The Persistence method considers the current frame as the nowcasted image while the SSD method tries to estimated the motion vector and applies it to the current image in order to compute the nowcasted image.

B. The First Group case studies results

The Table IV-1,Table IV-2 and Table IV-3 show the results of the ensemble nowcast model with respect to the Persistence and the SSD for the 30 minutes ahead nowcast.

Model/Channel	DAN	SSD	Persistence
Ch. 4	1.26	1.09	0.72
Ch. 5	0.15	0.09	-0.02
Ch. 6	0.28	0.22	-0.02
Ch. 7	0.72	0.64	0.25
Ch. 8	0.34	0.31	0.10
Ch. 9	0.77	0.68	0.27
Ch. 10	0.73	0.63	0.23
Ch. 11	0.44	0.39	0.11

Table IV-1. The BIAS mean values, in °K, computed on the three training case studies for the 30 minutes ahead nowcasted images : the values of the three models are comparable for each MSG channel.

Model/Channel	DAN	SSD	Persistence
Ch. 4	7.41	8.20	9.05
Ch. 5	2.24	2.41	2.72
Ch. 6	4.58	5.04	5.62
Ch. 7	9.19	10.12	11.11
Ch. 8	4.94	5.20	5.71
Ch. 9	9.61	10.57	11.62
Ch. 10	9.29	10.16	11.20
Ch. 11	6.01	6.62	7.35

Table IV-2. The RMSE mean values, in °K, computed on the three training case studies for the 30 minutes ahead nowcasted images : the values of the DAN model are better than the Persistence and the SSD models.

Model/Channel	DAN	SSD	Persistence
Ch. 4	89.50	87.05	84.40
Ch. 5	93.12	91.90	89.84
Ch. 6	92.63	91.09	89.15
Ch. 7	92.43	90.73	89.02
Ch. 8	92.34	91.60	89.99
Ch. 9	92.60	90.93	89.20
Ch. 10	92.84	91.27	89.55
Ch. 11	93.09	91.50	89.69

Table IV-3. The Correlation Index mean values, in %, computed on the three training case studies for the 30 minutes ahead nowcasted images : the correlation of the DAN model are better than the Persistence and the SSD models.

The Table IV-4, the Table IV-5 and the Table IV-6 show the results of the ensemble nowcast model with respect to the Persistence and the SSD for the 60 minutes ahead nowcast.

Model/Channel	DAN	SSD	Persistence
Ch. 4	1.80	1.99	1.94
Ch. 5	0.22	0.20	0.21
Ch. 6	0.40	0.46	0.45
Ch. 7	1.14	1.30	1.29
Ch. 8	0.50	0.62	0.58
Ch. 9	1.21	1.36	1.36
Ch. 10	1.14	1.28	1.28
Ch. 11	0.69	0.80	0.78

Table IV-4. The BIAS mean values, in °K, computed on the three training case studies for the 60 minutes ahead nowcasted images : the DAN values are better than the others, because the correlation between the images are lower at 60 Minutes. The SSD and the Persistence are more influenced by the correlation than the Ensemble.

Model/Channel	DAN	SSD	Persistence
Ch. 4	10.16	11.38	12.28
Ch. 5	3.30	3.38	3.79
Ch. 6	6.57	7.04	7.78
Ch. 7	13.11	14.16	15.40
Ch. 8	6.95	7.28	7.89
Ch. 9	13.77	14.83	16.13
Ch. 10	13.36	14.30	15.59
Ch. 11	8.74	9.35	10.25

Table IV-5. The RMSE mean values, in °K, computed on the three training case studies for the 60 minutes ahead nowcasted images : the values of the DAN model are better than the Persistence and the SSD models.

Model/Channel	DAN	SSD	Persistence
Ch. 4	79.55	74.62	70.84
Ch. 5	85.03	83.57	79.74
Ch. 6	85.01	81.84	78.45
Ch. 7	84.54	81.13	78.22
Ch. 8	84.89	82.91	80.30
Ch. 9	84.73	81.46	78.55
Ch. 10	85.12	82.09	79.18
Ch. 11	85.41	82.44	79.37

Table IV-6. The Correlation Index mean values, in %, computed on the three training case studies for the 60 minutes ahead nowcasted images : the correlation of the DAN model are better than the Persistence and the SSD models.

The Table IV-7, the Table IV-8 and the Table IV-9 show the results of the ensemble nowcast model on the validation case study with respect to the Persistence and the SSD for the 30 minutes ahead nowcast.

Model/Channel	DAN	SSD	Persistence
Ch. 4	0.75	1.11	0.97
Ch. 5	0.03	0.08	0.03
Ch. 6	0.10	0.15	0.06
Ch. 7	0.04	0.19	0.03
Ch. 8	0.09	0.21	0.06
Ch. 9	0.09	0.15	0.06
Ch. 10	0.09	0.21	0.06
Ch. 11	0.09	0.15	0.06

Table IV-7. The BIAS mean values, in °K, computed on the validation case study for the 30 minutes ahead nowcasted images : the DAN values are comparable with respect to the other models.

Model/Channel	DAN	SSD	Persistence
Ch. 4	9.28	10.7	10.94
Ch. 5	2.03	2.08	2.07
Ch. 6	5.07	5.59	5.69
Ch. 7	10.31	11.45	11.85
Ch. 8	4.19	4.21	4.37
Ch. 9	10.8	12	12.42
Ch. 10	10.54	11.66	12.03
Ch. 11	6.41	7	7.19

Table IV-8. The RMSE mean values, in °K, computed on the validation case study for the 30 minutes ahead nowcasted images : the values of the DAN model are better than the Persistence and the SSD models.

Model/Channel	DAN	SSD	Persistence
Ch. 4	78.23	73.54	71.58
Ch. 5	93.66	93.83	93.55
Ch. 6	85.83	83.81	82.64
Ch. 7	81.46	78.44	76.31
Ch. 8	81.64	83.03	80.71
Ch. 9	81.71	78.68	76.58
Ch. 10	82.12	79.38	77.39
Ch. 11	84.12	82.22	80.53

Table IV-9. The Correlation Index mean values, in %, computed on the three training case studies for the 30 minutes ahead nowcasted images : the correlation of the DAN model are better than the Persistence and the SSD models.

The above tables show that the model generalizes very well with respect to the SSD and the Persistence.
The latest tables show the results of the ensemble nowcast model on the validation case study with respect to the Persistence and the SSD for the 60 minutes ahead nowcast.

Model/Channel	DAN	SSD	Persistence
Ch. 4	1.4	1.57	1.47
Ch. 5	0.02	0.03	0.02
Ch. 6	0	0.06	0.01
Ch. 7	-0.31	-0.09	-0.19
Ch. 8	-0.23	-0.2	-0.24
Ch. 9	-0.33	-0.09	-0.19
Ch. 10	-0.24	-0.02	-0.11
Ch. 11	-0.11	0	-0.05

Table IV-10. The BIAS mean values, in °K, computed on the validation case study for the 60 minutes ahead nowcasted images : the DAN values are comparable with respect to the other models.

Model/Channel	DAN	SSD	Persistence
Ch. 4	11.13	12.65	12.88
Ch. 5	2.54	2.52	2.54
Ch. 6	6.04	6.66	6.77
Ch. 7	12.37	13.8	14.07
Ch. 8	12.69	14.09	14.35
Ch. 9	7.73	8.45	8.6

Ch. 10	12.69	14.09	14.35
Ch. 11	7.73	8.45	8.6

Table IV-11. The RMSE mean values, in °K, computed on the validation case study for the 60 minutes ahead nowcasted images : the values of the DAN model are better than the Persistence and the SSD models.

Model/Channel	DAN	SSD	Persistence
Ch. 4	66.22	62.81	60.48
Ch. 5	89.95	90.97	90.37
Ch. 6	78.63	77.09	75.42
Ch. 7	71.32	68.66	66.45
Ch. 8	71.81	75.28	73.02
Ch. 9	71.56	68.9	66.71
Ch. 10	72.15	69.93	67.77
Ch. 11	75.26	74.13	72.13

Table IV-12. The Correlation Index mean values, in %, computed on the three training case studies for the 60 minutes ahead nowcasted images : the correlation of the DAN model are quite better than the Persistence and the SSD models.

Like the 30 minutes results, the ensemble model shows to be more general than the SSD and the Persistence models and its performances indexes are very good.

C. The Second Group case studies results

In this section the rain field 30 and 60 minutes ahead nowcast reconstruction are presented.
The results belonging to the second group are related to the results of the first group, because the rain field are reconstructed using the MSG images nowcasted by the GenCAST model showed in the previous section.
The results are related to the GLM Cloud Mask performance and to the performance indexes used to measure the results of the GenCAST in the previous section.

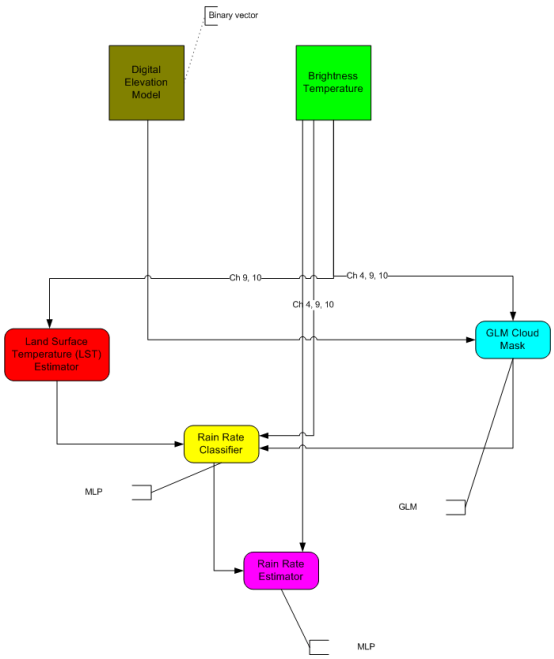

Fig. 8. The rate rate estimator layout. The 3 models used are the GLM for the Cloud Mask and the Multi Layer Perceptron [19] for the rain rate classifier and the rain rate estimator. A simple LST estimator [28] is used to get the background temperature and a DEM model is used in order to discriminate between the land and the sea pixels. The MSG channel used are showed on each edge.

The following contingency tables present the pixel Cloud/No-Cloud classification with respect to the Rain/No-Rain classification based on the MPE. The tables are related to the GLM Cloud Mask and to the Eumetsat Cloud Mask.

(Eumetsat ,GLM) CM	No Rain	Rain
No Cloud	(37776,56840)	(0,0)
Cloud	(49240,30176)	(7584,7584)

Table IV-13. The 2010/02/01 case study. The pixel rain classification of the Eumetsat Cloud Mask with respect to the MPE rain pixels. Each pair (Eumetsat CM,GLM CM) in each cell contains the number of pixel classification with respect to the Rain/No-Rain class.

(Eumetsat ,GLM) CM	No Rain	Rain
No Cloud	(2047,44544)	(0,1)
Cloud	(84880,42383)	(7673,7672)

Table IV-14. The 2010/01/26 case study. The pixel rain classification of the Eumetsat Cloud Mask with respect to the MPE rain pixels. Each pair (Eumetsat CM,GLM CM) in each cell contains the number of pixel classification with respect to the Rain/No-Rain class.

The Table IV-13 and the Table IV-14 show that the GLM Cloud Mask acts as a filter on the "No Rain" pixels. In fact the number of the "No Rain" Eumetsat CM pixels is more than the number of "No Rain" GLM CM pixels. The GLM CM can be used in place of the Eumetsat CM in order to filter the rain pixels. On this subset of pixels the rain rate classifier and the rain rate field estimator will be assessed.

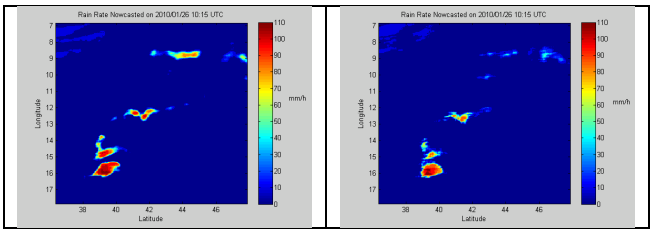

Fig. 9. The case study 2010/01/26: the 30 minutes nowcasted image (to the left) and the 60 minutes nowcasted image (to the right).

30 Minutes Nowcast	60 Minutes Nowcast
BIAS: 2.56 mm/h	**BIAS:** 1.33 mm/h
RMSE: 10.29 mm/h	**RMSE:** 9.05 mm/h
Correlation Index: 76.27%	**Correlation Index:** 68.47%

Table IV-15. The performance indexes computed on the 2010/01/26 case study: the RMSE is about 10% the MPE rain rate peak (110 mm/h).

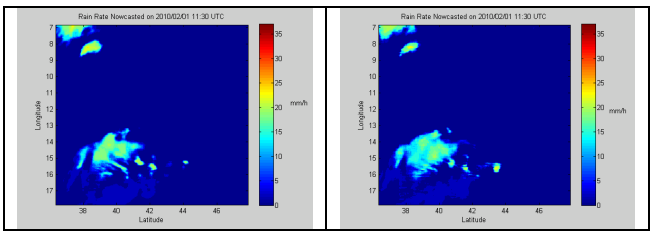

Fig. 10. The case study 2010/02/01: the 30 minutes nowcasted image (to the left) and the 60 minutes nowcasted image (to the right).

30 Minutes Nowcast	**60 Minutes Nowcast**
BIAS: 1.94 mm/h	**BIAS:** 2.03 mm/h
RMSE: 4.78 mm/h	**RMSE:** 4.97 mm/h
Correlation Index: 57.27%	**Correlation Index:** 50.27%

Table IV-16. The performance indexes computed on the 2010/01/26 case study: the RMSE is about 13% the MPE rain rate peak (37 mm/h).

The results show a good shape reconstruction of the rain rate field and a good performance indexes in terms of correlation and RMSE. The indexes on the 2010/01/26 case study are better because the rain event is a "Violent" [29] event like the 2010/09/08 (the training event).

V. Conclusions

In this work a new version of the NeuCAST model named GenCAST, based on the GLM model for the MSG images nowcasting has been presented. In the first part of the work has been showd the flexibility and the generalization of the GenCAST in terms of performances indexes with respect to the Persistence and the SSD. The results showed are related to the 30 minutes ahead and 60 minutes ahead nowcast. The indexes have shown that the model performs better than the other benchmarks and generalizes very well.

The second part of the work has shown the application of the GenCAST model, trained in the first part, in order to nowcast the rain rate field on two different case studies. The results have shown a good performance for the "Violent" [29] rain event as expected.

The GenCAST model should be used to produce a wide range of meteorological products or it can be used as a synthetic satellite source to feed NWP models or weather software libraries e.g. SAF [27].

The GenCAST model should be used in a deployed system for Civil Protection or ATC purposes, but it needs to be trained on a greater number of events in order to increase its accuracy.

Acknowledgment

Meteosat data has been provided by Eumetsat.

References

[1] G. Roth, G. Boni, F. Giannoni and R. Rudari, "On the role of a hydrologic model in regional precipitation and flood frequency analyses, EOS", *Trans.AGU*, vol. 85(17), JA259, 2004.

[2] F. Siccardi; G. Boni; L. Ferraris; and R. Rudari, "A hydrometeorological approach for probabilistic flood forecast", *J. Geophys. Res.*, Vol. 110, No. D5, D05101, 2004.

[3] L. Li, W. Schmid, and J. Joss, "Nowcasting of motion and growth of precipitation with radar over a complex orography," *J. Appl. Meteorol.*, vol. 34, pp. 1286–1300, June 1995.

[4] J. W. Wilson, N. A. Crook, C. K. Mueller, J. Sun, and M. Dixon, "Nowcasting thunderstorms: A status report", *Bull. Amer. Meteor. Soc.*, vol. 79, n. 10, pp. 2079-2099, 1998.

[5] F.S. Marzano, A. Mugnai and J. Turk, "Precipitation retrieval from spaceborne microwave radiometers and combined sensors", in *Remote ensing of atmosphere and ocean from space*, F.S. Marzano and G. Visconti Eds., Kluwer Academic Publ., Dordrecht (NL), pp. 107-126, 2002.

[6] G.A. Vicente, R.A. Cofield, and W.P. Menzel, "The operational GOES infrared rainfall estimation technique", *Bull. Amer. Meteor. Soc.*, vol. 9, pp 1883-1898, 1998.

[7] K.L. Hsu., X. Gao, S. Sorooshian and H.V. Gupta, "Precipitation estimation from remotely sensed information using artificial neural networks", *J. Appl. Meteor.*, vol. 36, pp. 1176-1190, 1997.

[8] C. Kummerow and L. Giglio, "A method for combining passive microwave and infrared rainfall observations", *J. Atmos. Oceanic Tecnol.*, vol. 12, pp. 33-45, 1995.

[9] V. Levizzani, F. Porcù, F.S. Marzano, A. Mugnai, E.A. Smith, and F. Prodi, "Investigating a SSM/I microwave algorithm to calibrate METEOSAT infrared instantaneous rain-rate estimates" *Meteor. Applications*, vol. 3, pp. 5-17, 1996.

[10] S.W. Miller, P.A. Arkin, and R. Joyce, "A combined microwave infrared rain rate algorithm", *Int. J. Remote Sensing*, vol. 22, pp. 3285-3307, 2001.

[11] T. Bellerby, M. Todd, D. Kniveton and C. Kidd, "Rainfall Estimation from a Combination of TRMM Precipitation Radar and GOES Multispectral Satellite Imagery through the Use of an Artificial Neural Network", *J. App. Meteor.*, vol. 39, pp. 2115-2128, 2000.

[12] F.J. Tapiador, C. Kidd, V. Levizzani, and F.S. Marzano, "A neural networks-based PMW-IR fusion technique to derive half hourly rainfall estimates at 0.1° resolution", *J. Appl. Meteor.*, vol. 43, pp. 576-594, 2004.

[13] D.I.F. Grimes, E. Coppola , M. Verdecchia, G. Visconti, "A neural network approach to real time rainfall estimation for Africa using satellite data", *J. Hydrometeorology*, 6, 4, 1119-1133, 2003.

[14] F.S. Marzano, M. Palmacci, D. Cimini, G. Giuliani and J.F. Turk, "Multivariate statistical integration of satellite infrared and microwave radiometric measurements for rainfall retrieval at the geostationary scale", *IEEE Trans. Geosci. Remote Sens.*, vol. 42, n. 4, pp. 1018-1032, 2004a.

[15] R.R. Ferraro,"SSM/I derived global rainfall estimates for climatological applications", *J. Geophys. Res.*, vol. 102, pp 16,715- 16,735, 1997.

[16] S. Di Michele, A. Tassa, A. Mugnai, F.S. Marzano, P. Bauer and J.P.V. Poiares Baptista, "Bayesian Algorithm for Microwave-based Precipitation Retrieval: description and application to TMI measurements over ocean", *IEEE Trans. Geosci. Rem. Sens.*, vol. 43, pp. 778-791, 2005.

[17] F. Dell'Acqua and P. Gamba, "Pyramidal Rain Field Decomposition Using Radial Basis Function Neural Networks for Tracking and Forecasting Purposes", *IEEE Transactions on Geosci. and Remote Sensing*, vol. 41, no. 4, pp. 2003 853, 2003.

[18] G. Rivolta, F.S. Marzano, E. Coppola, and M. Verdecchia, "Artificial neural-network technique for precipitation nowcasting from satellite imagery", *Adv. in Geosci.*, vol. 7, pp. 97-103, 2006.

[19] Bishop C. M., *Neural Networks for Pattern recognition*, Oxford Press 1995, ISBN 0-19-853864-2

[20] T. Heinemann, A. Latanzio.,F. Roveda, The Eumetsat multi-sensor precipitation estimate (MPE), *Proceedings of the second International Precipitation Working Group (IPWG) meeting*, Madrid, Spain, September 2002.

[21] L. Cao, *Practical method for determining the minimum embedding dimension of a scalar time series*, Physical Review D, pp. 43-50, Dec. 1997.

[22] I. T. Jolliffe, (1986). Principal Component Analysis. *Springer-Verlag*. pp. 487. ISBN 978-0-387-95442-4..

[23] P. McCullagh, J. Nelder (1989). Generalized Linear Models, *Second Edition. Boca Raton: Chapman and Hall/CRC*. ISBN 0-412-31760-5.

[24] D. J. C. MacKay, A Practical Bayesian Framework for Backpropagation Networks, *Neural Computation*, vol.4 n°.3 pp. 448-472, 1992.

[25] F. S. Marzano, G. Rivolta, E. Coppola, B. Tomassetti, M. Verdecchia , Rainfall Nowcast from Multi-Satellite Passive Rainfall Nowcast from Multi-Satellite Passive, *TGRS-2006-00435*.

[26] Imran Maqsood et al., An ensemble of neural networks for weather forecasting, *Neural Comput & Applic* Vol. 13 pp. 112–122, 2004.

[27] www.nwcsaf.org

[28] M. Romaguera, J.A. Sobrino, G. Sria, M.M. Zaragoza, J. Cuenca, M. Gmez, J.C. Jimenez-Muñoz, A. Galdon-Ruiz, Land Surface

Temperature Derived from the MSG-SEVIRI Data, *Proceedings Second MSG RAO Workshop*, Salzuburg, Austria, 9-10 Sept. 2004.

[29] Met Office, National Meteorological Library and Archive, Fact Sheet N°3, Water in the Atmosphere, August 2007.